ACS APPLIED MATERIALS & INTERFACES

Research Article

www.acsami.org

Synergy between Graphene and Au Nanoparticles (Heterojunction) towards Quenching, Improving Raman Signal, and UV Light Sensing

María C. Dalfovo,[†] Gabriela I. Lacconi,[‡] Mónica Moreno,[§,⊥] Marta C. Yappert,[§] Gamini U. Sumanasekera,[∥] Roberto C. Salvarezza,[†] and Francisco J. Ibañez*[,†]

[†]Instituto de Investigaciones Fisicoquímicas, Teóricas y Aplicadas (INIFTA), Universidad Nacional de La Plata, CONICET, Sucursal 4 Casilla de Correo 16, 1900 La Plata, Argentina

[‡]INFIQC−CONICET, Dpto. de Fisicoquímica, Facultad de Ciencias Químicas, Universidad Nacional de Córdoba, Ciudad Universitaria, 5000 Córdoba, Argentina

[§]Department of Chemistry, University of Louisville, Louisville, Kentucky 40292, United States

[∥]Department of Physics and Astronomy, University of Louisville, Louisville, Kentucky 40292, United States

Supporting Information

ABSTRACT: Here, we developed a simple method for obtaining a heterojunction composed of graphene (G) and surfactant-coated Au nanoparticles (NPs) to measure film conductivity and surface enhanced Raman scattering (SERS). Monolayer G is obtained by chemical vapor deposition (CVD) and transferred via poly(methyl methacrylate) (PMMA) to microfabricated Au electrodes, glass, and silicon. Post-synthesis treatments of G with PMMA and ozone (O_3) showed 1 and 6 orders of magnitude decrease in film conductivity, respectively. The heterojunction formation with Au NPs had no major effect on G conductivity. In this work is demonstrated that G quenches more than 90% of the combined photoluminescence and fluorescence of Au NPs and Rhodamine B (RhB), respectively. Signal quenching permitted quantitative analysis of SERS of RhB on various substrates including as-transferred graphene, oxidized graphene (OG), and the heterojunction. While G is mainly responsible for quenching photoluminescence and fluorescence, ∼3 orders of magnitude increase SERS activity for RhB was accomplished by the heterojunction. Finally, we wanted to correlate changes in film current during UV light sensing experiments. We found striking differences in the sensing profiles at different UV energies.

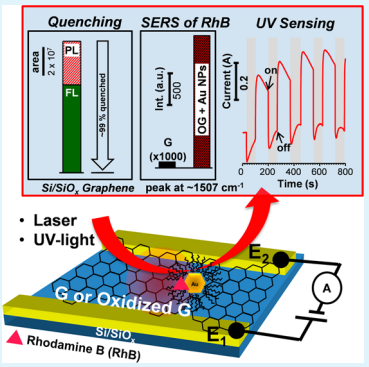

KEYWORDS: *graphene, nanoparticles, heterojunction, surface enhanced-Raman scattering, quenching, photoluminescence, and fluorescence*

INTRODUCTION

Graphene is a material comprised only of surface carbon atoms organized in a sp^2 honeycomb lattice. The unique chemical and electronic properties of graphene (G) have been employed towards sensing,[1] photonics,[2] optoelectronics,[2] and surface enhanced Raman scattering (SERS)[3] applications, to mention just a few. Graphene was initially isolated by mechanical exfoliation from graphite using scotch tape.[4] Later, other methods were developed for obtaining G including Hummers,[5] electrochemistry (electroexfoliation),[6] and chemical vapor deposition (CVD).[7] The CVD approach is simple and allows control on the size of G[7] however, the transferring protocol involves the use of poly(methyl methacrylate) (PMMA). PMMA is a polymer widely used in clean room laboratories during photolithography and in the construction of graphene field-effect transistors (G-FET).[8] Some researchers have used PMMA as a protecting layer against oxidation with ozone (O_3)[9] and during the detection of volatile organic compounds (VOCs).[10] Despite these advantages, PMMA usually remains as a residue in the G film. Ruoff and co-workers[11] demonstrated the presence of PMMA on CVD grown graphene by comparing XPS plots before transferring (graphene on Cu), after transferring, and after thermal annealing. They determined that after transferring and annealing, the C 1s peak never returned to the original sp^2 configuration indicating the presence of PMMA residues on the G film. Other groups also employed different approaches to completely remove PMMA from as-transferred G.[12−14] In line with the above, we found that PMMA lowered G current altering its electronic properties. The presence of PMMA on the G film is not trivial and it should be considered during device fabrication, SERS,[14] and sensing[8] applications.

Raman scattering has a very low cross section $\sim 10^{-31}$ cm^2 per molecule, and unevenly competes with fluorescence (FL) whose probability of occurring is much higher ($\sim 10^{-16}$ cm^2 per molecule). Low molecule polarization in Raman scattering has been overcome by a surface phenomena known as surface enhanced Raman scattering (SERS).[15] Once Raman active

Received: December 13, 2013
Accepted: April 21, 2014

   dx.doi.org/10.1021/am405753t | ACS Appl. Mater. Interfaces XXXX, XXX, XXX−XXX

molecules locate nearby highly confined electromagnetic spots, an electromagnetic[16] and/or chemical[17] enhancement may occur carrying out the former the greatest signal enhancement (10^{14}). Since its discovery in 1970,[15] researchers have been pursuing new nanomaterials for improving SERS activity. For instance, extremely low analyte concentrations have been detected[18] even down to a single molecule detection.[19] Metal nanostructures of various composition, size, and shape employed in SERS are usually obtained by electrodeposition,[20,21] photolithography and sputtering,[22] and bench-top chemical synthesis.[23] Although the actual mechanism is still unclear, the composition, shape, and size seem to play a crucial role in SERS. One example are anisotropic nanoparticles (Ag NPs) that posses a stronger enhancement over spherical ones as demonstrated between sharp and truncated Ag nanocubes.[24] Also, the composition plays a crucial role, which has led to the use of Ag over Au nanostructures. However, there are some drawbacks associated with the use of those nanostructures in SERS due to the propensity of Ag to oxidize at ambient conditions. As expected, oxidation of metallic nanostructures with sharp tips not only changes the composition but also leads to the loss of hot-spots by the formation of rounded features (i.e., from nanoplates to nanoparticles).[25] The incorporation of metal nanoparticles (NPs) onto graphene is known to improve SERS however, it has been demonstrated that photoluminescence (PL) intensity becomes an issue for nanoparticles ~5 nm.[26] In addition, some active molecules may undergo fluorescence (FL) during laser excitation in Raman experiments.[27] Those undesired effects (i.e., oxidation of metal nanostructures, PL, and FL) are detrimental to SERS because of loss of hot spots and overlapping of the analytical signal.

At first glance, G seems to satisfy all the requirements for SERS due to a vast surface area, delocalized electrons, ability to charge transfer, and biocompatibility. All of those attributes are true, however, CVD grown G has demonstrated poor Raman enhancement of various analytes.[9] Recently, Hou and co-workers compared exfoliated graphene with reduced graphene oxide (rGO).[28] By controlling the degree of reduction of rGO, 1-fold increase in SERS activity of Rhodamine B (RhB) was achieved. Later, Nam and co-workers exposed CVD grown G to UV-generated ozone and observed ~1 order of magnitude improved SERS activity of RhB, Rh6G, and crystal violet.[9] Liu et al. initially formed a heterojunction with Cu NPs and exfoliated G followed by dissolving the Cu NPs in order to construct a nanomesh. This approach created several defects (hot spots) within the G film ultimately resulting in ~1.8 enhancement factor (EF) of RhB.[29] Some groups have further improved SERS activity by incorporating metal nanoparticles as a co-enhancer.[30−33] For instance, Murphy et al.[30] reduced Ag^+ in the presence of graphene oxide (GO) in order to form GO-Ag nanoparticles composite. This elegant approach allowed the detection of 140 nM porphyrin derivatives. Following a similar procedure, Dutta et al. reduced Ag ions in the presence of GO achieving a limit of detection (LOD) as low as 10 nM of uranyl acetate.[31] Others adsorbed Ag/Au alloy nanoparticles onto functionalized GO, which exhibited ~1.5 orders of magnitude improved SERS activity of Alexa fluor 488 as compared to GO alone.[32] Just recently, Min and co-workers sandwiched organic-coated Ag nanoparticles by placing the film between reduced graphene oxide (rGO) at the bottom and GO at the top. This approach prevented oxidation of Ag nanoparticles for more than two months while improving SERS activity of Rh6G by ~1.6-fold.[33]

In this report, we developed a simple method for obtaining a heterojunction with G and surfactant-coated Au NPs via hydrophobic interaction between both films. Although the use of organic-coating surrounding the Au cores imparted stability and allowed the formation of the heterojunction, the alkyl chains had to be removed by thermal treatments. We explored into conductivity and Raman (SERS) of as-transferred graphene (G), oxidized graphene (OG), and the heterojunction (Au NPs decorating either G or OG). We observed an interesting synergy between both films upon quenching PL and FL, and improving SERS activity. We encountered that as-transferred graphene suppressed most of the undesired PL and FL meanwhile, Au NPs acted as a co-enhancer of RhB. Since π-electrons in nanocarbons rule conductivity, we were curious about the effect of different UV light energies on the electronic properties of graphene.[34] These results may have important implications in the construction of G-FET, SERS, and solar panels.

EXPERIMENTAL SECTION

Synthesis of Au NPs and Graphene. The TOABr-coated Au NPs were synthesized according to the two-phase Brust-Schiffrin reaction but without the addition of alkanethiols as reported.[35] The NPs prepared this manner are 4.39 ± 1.25 nm diameter according to TEM.[36] Graphene was grown in a Cu foil and transferred to various substrates following a protocol reported somewhere else.[37] The samples were transferred to Au microelectrodes separated either by 5 μm (interdigitated Au electrodes, IDA shown at the Inset in Figure

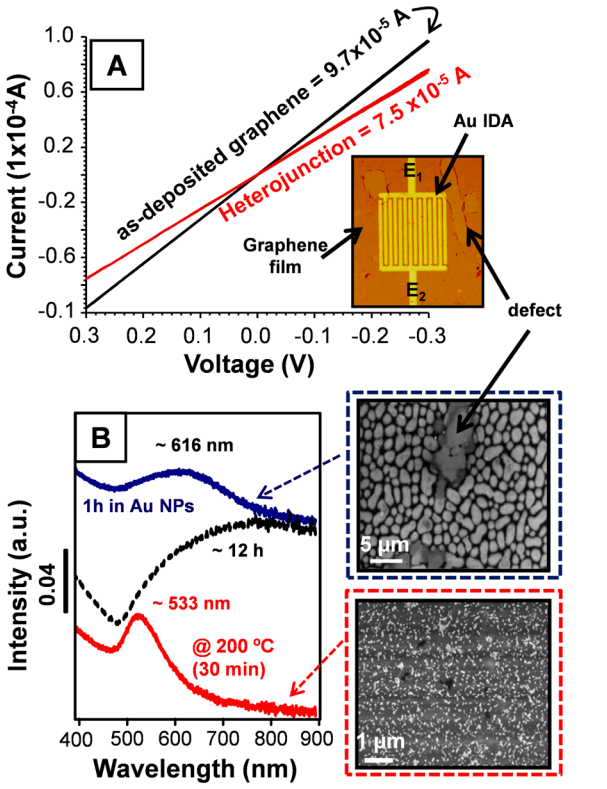

Figure 1. Plot of current vs potential ($I-V$) curves for as-transferred graphene (G) onto microelectrodes and after 1 h immersed in TOABr-Au NPs solution (A) and UV−vis spectra of as-transferred G on glass immersed into TOABr-Au NPs solution for 1 and 12 h, and after heating the film at 200 °C along with SEM images taken at the indicated times (B).

dx.doi.org/10.1021/am405753t | ACS Appl. Mater. Interfaces XXXX, XXX, XXX−XXX

1A) or 23 μm for conductivity measurements. Glass and Si substrates were employed in LSPR and SERS experiments, respectively.

Film Post-treatments. In order to clean as-transferred G, samples were immersed in worm acetone for removing PMMA followed by rinsing with various solvents and drying under N_2 flow. Oxidation of graphene was performed in an UVO ozone cleaner (Jelight Company Inc., Irvine, CA) at different time intervals. The heterojunction was formed either on graphene or oxidized graphene films accomplished by immersing both films into Au NPs solution for 1 and 12 h. Drop-cast Au NP films were drop-casted from 10 μL Au NPs (1.4-1.6 mg/μL concentration) solution onto Si and SiO_x substrates. Thermal treatment was acquired in a Barnstead/Thermolyne Small Benchtop Muffle Furnaces Type 1300 (Thermo Scientific) at 200 °C for 30 min.

Films Characterization. Films were characterized by XPS using an Mg KR source (XR50, Specs GmbH) coupled to a hemispherical electron energy analyzer (PHOIBOS 100, Specs GmbH). UV−vis spectroscopy was acquired in a PerkinElmer Lambda 35 Spec. in a wavelength range between 300 and 900 nm. The heterojunction was formed on glass and films were run at ambient conditions. FTIR spectra were acquired on a PIKE Miracle Varian 600 Instrument in transmission mode and performed in clean glass before and after addition of few drops of diluted PMMA in toluene. SEM images of the heterojunction were acquired on a FEI QUANTA 400 between 15-20 keV. AFM images were acquired with a Veeco Digital Instruments Nanoscope V (Santa Barbara, CA) using a Si tip operating in tapping mode. Samples used for AFM were assembled and thermally treated following the same protocol described below. Thermogravimetric analysis (TGA) was acquired on NETZSCH STA 409C in a temperature range between 30 and 500 °C. Nanoparticles powder (50 mg) was placed in an alumina crucible and heated for 10 min in an oxidizing air at intervals of 10 °C.

Raman Experiments. Raman spectra were acquired in a LABRAM-HR Horiba Jobin-Yvon confocal microscope Raman system with a 100× objective lens with numerical aperture (NA) of 0.9. The laser excitation and power employed was 632.8 nm (He−Ne) and 1.7 mW, respectively. Low laser power was used in order to avoid laser-induced heating. During SERS experiments, 20 μL (2.0 x 10^{-5} M) of RhB aqueous solution (pH = 5) was drop-coated onto Si, SiO_x, as-transferred G, and OG, and films were allowed to dry for 1 h.

Conductivity Measurements and UV Sensing. Solid-state electronic conductivity and sensing measurements were acquired in a CH Instruments 700D Bipotentiostat (Austin, TX) electrochemical workstation. Current was measured on graphene films across interdigitated electrodes (IDA) or electrodes having a 23 μm gap. The electrodes were fabricated in a clean room by photolithography on a Si/SiO_x substrate (INTI, Argentina). Wire leads were attached to the electrode contact pads with Ag epoxy (cured 12 h, 80°C), which was further insulated with an overlayer of torr-seal epoxy (cured 12 h, 80 °C). The electrode was cleaned by immersion in anisole and dichloroethane followed by rinsing in acetone, ethanol, and isopropanol, and drying under N_2. One electrode was connected to the reference and counter electrode leads while the other electrode was connected to the working electrode lead. Sensing experiments were performed in chronoamperometry mode (CA). The current was monitored with time while a 0.3 V potential was applied between the two electrodes and the sample was exposed to "on/off" cycles of UV light applied at different energies. The highest energy lamp was obtained with the UVO cleaner operating at 180 nm (for generating highly reactive species) and 254 nm for oxidation of the organic material. Two other Hg lamps operating at 254 and 365 nm (6 W/cm^2 power intensity) were also used for comparing UV sensing profiles. Ultraviolet (UV) illumination lamp was kept at 15 cm from the samples. All the experiments were conducted at ambient conditions.

RESULTS AND DISCUSSION

Heterojunction Formation. The heterojunction was simply formed by dipping as-transferred G into the toluene-containing surfactant-coated Au NPs. Figure 1A shows a plot of current as a function of potential ($I-V$ curves) before and after forming the heterojunction on interdigitated Au electrodes (IDA) indicating small changes in conductivity. The potential window applied for all the samples under study varied from −300 to 300 mV. High quality monolayer G (See Figure S1 and S2 in Supporting Information) exhibits ohmic current ∼9.7 × 10^{-5} A (at 300 mV) in close agreement with measured conductivity reported in the literature.[8] On the basis of graphite conductivity ($\sigma \sim 5.3 \times 10^{-5}$ ohm.cm) reported by Wallace,[38] we calculated[39] film current across 5 μm gap on IDA Au microelectrodes shown in the inset in Figure 1A. The calculated current exhibited ∼0.4 A, which is generally 4 to 5-fold higher current than the conductivity measured in our devices. We believe that remaining PMMA and defects along the film (cracks or voids as observed in Figure 1A) are responsible for the decreased in film conductivity. Supporting Information Figure S3 shows a complete characterization by means of XPS, Raman, conductivity, optical images (refractive index), and FTIR of as-transferred and post-treated G.

Figure 1B includes UV−vis spectra of a selected heterojunction (TOABr-Au NPs and G) formed on a clean glass substrate. After 1 h dipping the graphene film into Au NPs solution, the plasmon band appeared broad and red shifted (by ∼80 nm) as compared with the same NPs on glass,[36] whereas overnight immersion (∼12 h) resulted in no plasmon absorbance, consistent with NPs agglomeration and purple-looking film (not shown). Interestingly, just 1 h immersion showed islands composed of agglomerated NPs in the form of micelles[40] within the entire image except for the defects. After thermal treatment, the plasmon band blue shifted from ∼620 to 530 nm and sharpened. In addition, the film turned reddish (not shown) consistent with SEM images, which exhibits a more spread out configuration of Au NPs or islands. Both the blue shifting and sharpening of the plasmon band are attributed to a combination between film restructuring (separation between NPs)[41] and loss of organic material. The latter lowers the refractive index (RI)[42] leading to a blue shift and an improvement of plasmon intensity[43] as clearly noted in Figure 1B. We performed the same experiment using another transparent/conductive electrode such as indium tin oxide (ITO) in order to compare both substrates. Unlike G, ITO electrode required functionalization, longer immersion times in NPs solution (∼12 h), and thermal treatment for slightly improving the plasmon intensity as shown in Supporting Information Figure S4.

Photoluminescence (PL) Quenching by Graphene. Before performing SERS of Rhodamine B (RhB) on G, we wanted to characterize the heterojunction by means of Raman spectroscopy. Figure 2A and B compare Raman spectra of Au NPs deposited on Si and on G (heterojunction) before and after thermal treatment, respectively. Few interesting aspects should be considered as follows. First, the Si band at ∼958 cm^{-1} (marked with *) became completely shielded by a broad and intense spectrum arising from the Si/Au NPs film after thermal treatment (Figure 2B). The shaded area under the spectrum indicates photoluminescence (PL) calculated by the difference between the integrated area under the spectrum and the area under the peaks after baseline correction (Supporting Information Figure S5 shows an example of the calculated PL area). Second, the band at ∼2885 cm^{-1} attributed to C−H symmetric stretching displayed, after heating, more than 1 order of magnitude greater SERS activity. Finally, it is noticeable the ability of graphene to suppress 93% of PL as indicated in the bar chart in Figure 2C.

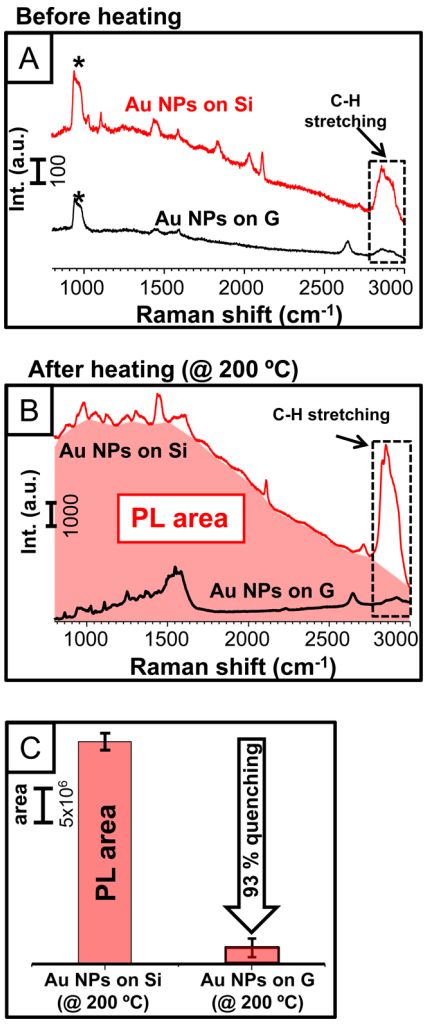

Figure 2. TOABr-Au NPs decorating Si (100) and G (heterojunction) before (A) and after (B) heating at 200° C for 30 min, and a bar chart indicating the percent photoluminescence (PL) quenched by G calculated by the area under the curve for two different samples (C). Raman plots in A are offset for better comparison.

Although the organic layer surrounding Au NPs imparted stability and allowed the formation of the heterojunction via hydrophobic interaction, it is known that alkyl chains may diminish the SERS signal.[44] Accordingly, both samples were heat treated with the aim of removing the organic shell. Supporting Information Figure S6 shows TGA and FTIR experiments indicating that TOA^+ ligands started desorbing at ~150 °C and most of the organic material was removed (~98%) at 200 °C after the indicated time, respectively. The removal of organics led to some considerations. It is known that illumination on naked Au or Ag films may cause photoluminescence (PL).[45] This phenomenon has been previously observed on Au thin films[46] and nanoparticles[26] during Raman experiments. In our experiments, PL appeared after sample heating as clearly noted by the large intensity shown in Figure 2B. One reason for such a large PL intensity could be associated with the loss of alkyl chains and nanoparticles annealing.[47,48] Consistent with the latter, we observed an increase in the root mean square (RMS) roughness from ~4 to 8 nm after heating the heterojunction. AFM images (Supporting Information Figure S7) exhibited larger and well-defined NPs or islands after thermal treatment consistent with SEM in Figure 1B. It should be noted that the laser energy of 633 nm falls within the plasmon absorption range (~530 to 620 nm) as shown in Figure 1B. Therefore, the significant suppression of PL could be attributed to a resonance energy transferred from Au NPs to G at the heterojunction as recently demonstrated to occur for Au nanorods.[49]

Synergy between Graphene (G) and Oxidized Graphene (OG) in the Heterojunction. In this section, we explored into the synergetic behavior of the heterojuntion towards SERS of RhB. Scheme 1 represents all the steps at which G and oxidized graphene (OG) were subjected during Raman experiments. SiO_x substrates were used for comparison. Figure 3A compares Raman spectra of RhB adsorbed on SiO_x and G. RhB peaks were indicated with (*) and appeared mounted on an intense spectrum. The shaded area under the spectrum corresponds to fluorescence (FL) evolved from RhB and calculated the same manner as PL in Figure 2B (see Supporting Information Figure S5 for details). The inset in Figure 3A shows a zoom-in spectrum of RhB on G in a range

Scheme 1. Raman Experiments Performed during the Construction of the Heterojunction

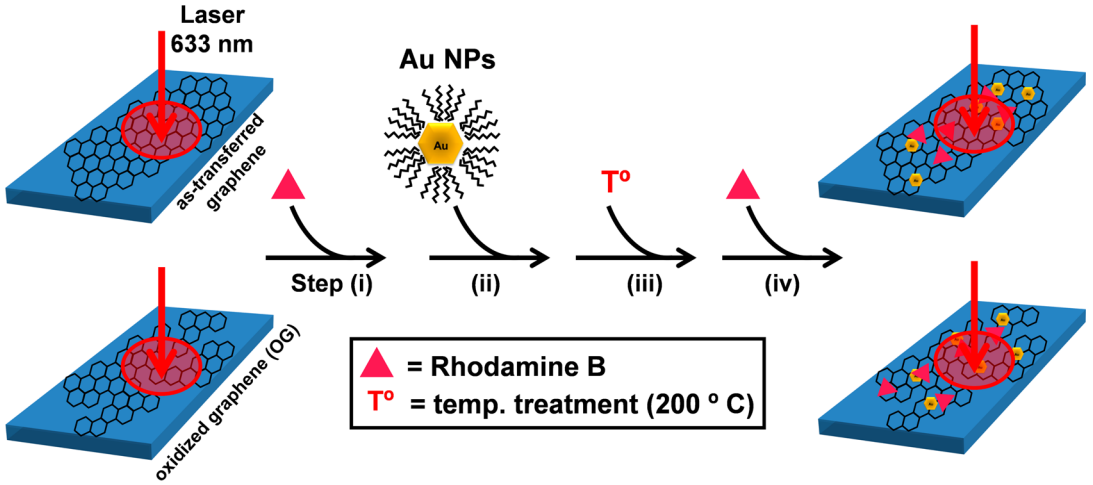

Raman experiments performed on graphene (G) and oxidized graphene (OG) subjected to different treatments as indicated. Note that Rhodamine B is added twice due to desorption of the analyte after thermal treatment.

dx.doi.org/10.1021/am405753t | ACS Appl. Mater. Interfaces XXXX, XXX, XXX–XXX

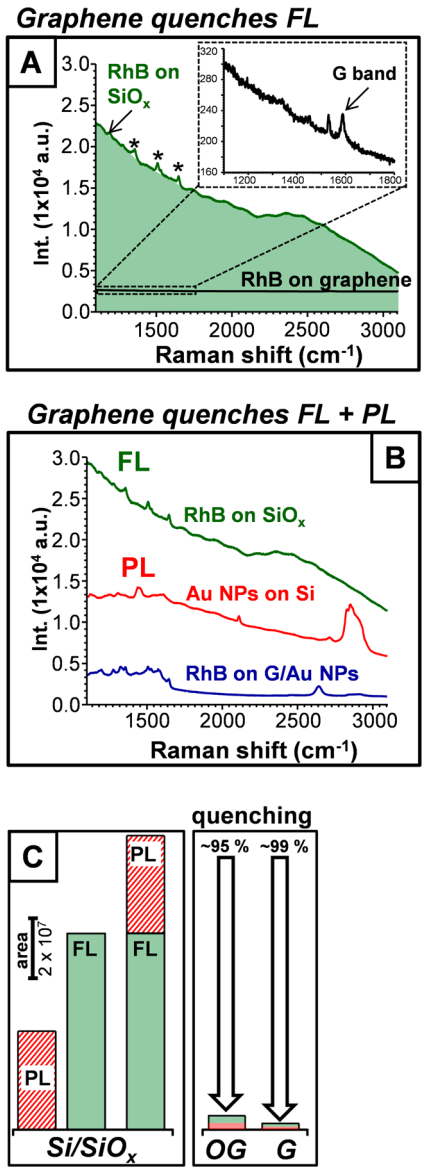

Figure 3. Raman plots of Rhodamine B (RhB) on SiO_x and on as-transferred G (A), RhB on SiO_x, PL spectrum taken from Figure 2B, and RhB on the heterojunction (Au NPs and G) as indicated (B), and bar char indicating quenching of PL and FL by OG and G (C). Characteristic RhB peaks are indicated with *. Spectra in part B are offset for better comparison.

between 1100 and 1800 cm^{-1}. The inset shows two Raman peaks that correspond to the G band of graphene and the presence of PMMA (vide supra). This indicates that as-transferred G lacks of SERS activity due to the absence of RhB bands, which should have been appeared despite the large FL intensity. Figure 3B exhibits FL (from Figure 3A) and PL (from Figure 2B) spectra corresponding to RhB and Au NPs, respectively along with RhB adsorbed on the heterojunction. Both, PL and FL spectra are shown together in order to stress on the ability of G to suppress both effects. It should be mentioned that, although characteristic peaks of RhB at the heterojunction are not well-defined, FL and PL were greatly diminished by graphene. The bar chart shows quenching of 95% and 99% by OG and G in the heterojunction, respectively. The actual Raman spectrum corresponding to OG is not shown due to clarity purposes.

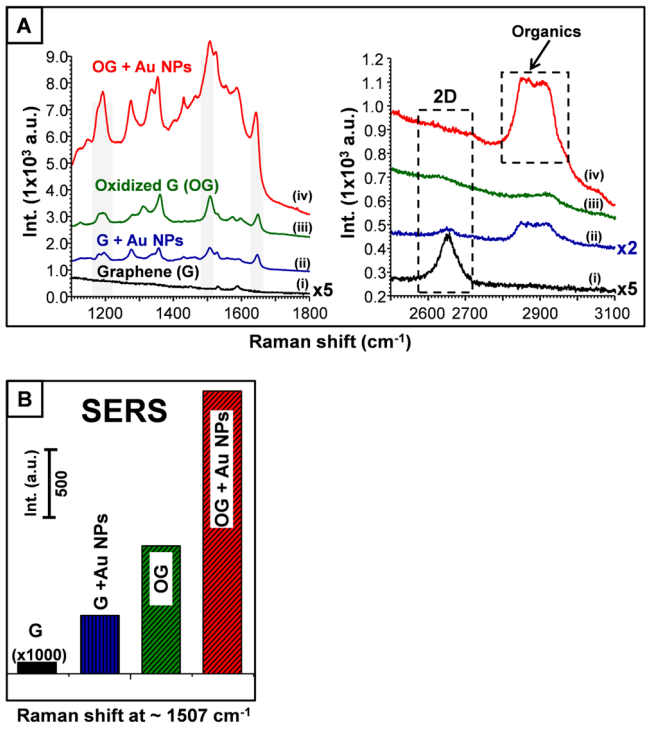

Figure 4. Selected Raman spectra of RhB on as-transferred G (i), heterojunction formed with Au NPs on G (ii), oxidized graphene (OG) (iii), and the heterojunction formed with Au NPs on OG (iv) (A) and a bar chart indicating SERS activity of RhB (at ~1507 cm^{-1}) at each step as noted (B). Plots are off set for better comparison.

Figure 4A exhibits selected Raman spectra of RhB obtained from the same area at each different step as indicated in Scheme 1. The spectra are separated into two panels for clarity. On the left and right panels are shown SERS activity and the characterization of the films by looking at the 2D and the C−H stretching bands, respectively. It is clear from the left panel that as-transferred G (i) is a poor Raman enhancer as noted by the absence of characteristics RhB peaks at 1195, 1507, and 1646 cm^{-1} (vide supra). Second, after the incorporation of Au NPs to G (ii), SERS activity was improved almost 2 orders of magnitude. It has been recently demonstrated that oxidization of CVD grown G dramatically improves Raman signal of various analytes.[9] Accordingly, we exposed G to UV-generated ozone (O_3) (see Supporting Information section S8 for more details). For instance, the bar chart in Figure 4B shows that OG alone (iii) exhibited better SERS activity than Au nanoparticles on as-transferred G (ii). Finally, once the OG film is decorated with Au NPs (iv) there is more than 3-fold increase in intensity of RhB with respect to as-transferred G alone (i) measured at 1507 cm^{-1}. On the right panel, as expected after oxidation and heating, the 2D band is missing and the C−H asymmetric peak is best seen, respectively. These results are consistent with the literature[9] and our data. In summary, Au NPs improve SERS activity of RhB however; the optimal enhancement was achieved by the heterojunction formed with OG (iv).

The bar chart in Figure 4B shows SERS of RhB at ~1507 cm^{-1} of the same selected sample before and after each step indicated in Scheme 1. Table 1 shows statistics obtained from two different spots within the same sample and measured at the three characteristics peaks of RhB as indicated. The Table shows an enhancement factor (EF) and the actual contribution

dx.doi.org/10.1021/am405753t | ACS Appl. Mater. Interfaces XXXX, XXX, XXX−XXX

Table 1. Average Relative Intensity of RhB, Enhancement Factor (EF), and Percent (%) SERS Contribution of Each Nanomaterial

films	avg. relative intensity and standard deviation of RhB at ~1195 cm^{-1}	~1507 cm^{-1}	~1646 cm^{-1}	peaks average[d]	EF[e]	% SERS contribution Au NPs	Graphene
graphene (G)[b,c]	0.067*	0.092*	0.074*	0.077	O×		100
G + AuNPs[b,c]	3.5 ± 0.6	3.1 ± 0.2	2.4 ± 0.1	3.0	41×	97	3
oxidized G (OG)[b,c]	2.3 ± 0.1	6.4 ± 1.5	3.9 ± 0.9	4.2	57×		100
OG + Au NPs[b,c]	5.5 ± 0.6	6.1 ± 0.7	5.8 ± 1.0	5.8	78×	28	72

[a]Note: average relative Raman intensity of RhB taken at two different areas within the same sample and measured at 1195, 1507, and 1646 cm^{-1}, enhancement factor (EF), and percent SERS contribution of each film involved in this study. * indicates the average intensity value without standard deviation because as-transferred graphene exhibited only one observable RhB signal from a pool of 7 samples. [b,c]Corresponds to the relative Raman intensity of RhB peak with respect to ~1589 and ~1128 cm^{-1}, taken on the same spectrum, respectively. [d]Average from all RhB peaks. [e]Enhancement factor (EF) indicates as many times RhB intensity was enhanced with respect to as-transferred graphene.

to SERS from each film involved in this study. The Table indicates that the heterojunction formed with as-transferred G, Au NPs are the main responsible in SERS activity. Nevertheless, when the heterojunction is formed with OG, the presence of Au NPs played a minor role contributing only to ~28% of the total SERS. In conclusion, there is an interesting synergy between both films towards SERS and the degree of enhancement depends on whether Au NPs are present and G oxidized.

UV Light Sensing. We finally wanted to explore into the effects of ultraviolet light (UV) on G. It has been demonstrated[50] and later corroborated by us (Supporting Information Figure S9) that the D and 2D band shift and the degree of change varies on the laser energy applied during Raman experiments. Since the 2D band is associated with π-electrons cloud, which controls the electronic properties of graphene, we were curious about the effect of UV light on film conductivity. Figure 5 displays a plot of current as a function of time (chronoamperometry, CA) for various substrates subjected to −0.3 V and exposed to 254 nm UV light during on/off periods of 100 s as indicated. The Figure shows experiments performed on SiO_x and bare microelectrodes (Si/SiO_x/Au electrodes) because they constitute the platform. As-transferred G films upon illumination displayed a decrease in conductivity and incomplete recovery during "on" and "off" cycles, respectively. As a control experiment, we covered the lamp in order to determine potential effects caused by generated O_3 inside the chamber.[9] Results indicated that transient exposure to O_3 have no effect on conductivity. We mechanically exfoliated few layers G (FLG) from HOPG and transferred them onto microelectrodes. Although, the exfoliated film showed similar conductivity to G there was no detectable response upon UV illumination. This experiment shed light onto the size-dependent properties of carbon materials.[51]

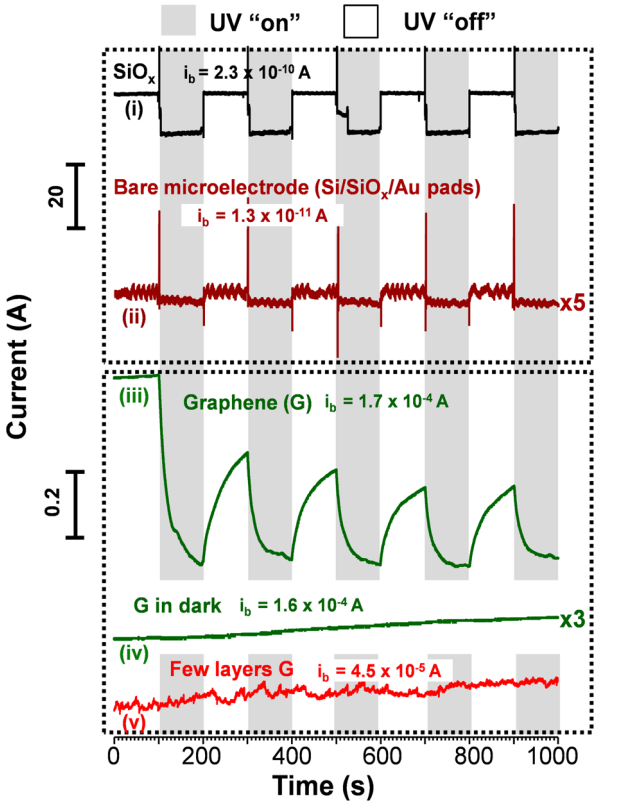

Figure 5. Chronoamperometry, CA (current vs time) plots of bare SiO_x (i), bare Au microelectrodes (Si/SiO_x/Au pads) (ii), as-transferred G on microelectrodes (iii), G in dark (iv), and few layers G transferred from scotch tape to microelectrodes (v) along with their corresponding baseline currents (i_b) as indicated. Plots are offset for better comparison.

At this point, the sensing mechanism remains uncertain but may involve photo-desorption of already adsorbed molecules when the film is illuminated.[52] It has been determined that moisture and O_2 readily adsorb on carbon withdrawing electrons from the film and turning it into a p-type material (majority of hole carriers).[11,53] The sensing mechanism has been explained as O_2 desorption from the film upon UV exposure. The observed decrease in film conductivity was attributed to a decrease of hole carries in the film caused by desorption of O_2 molecules.[54] As long as the UV lamp is turned off, O_2 species re-adsorb on G leading to an increase in conductivity. This sensing behavior has been previously observed in nanocarbon materials including semiconducting single-walled carbon nanotubes (SWNTs),[52] hybrid C60−Au nanoparticles,[55] and CVD grown G.[54,56] In general terms, all those reports have something in common: relatively fast current response upon illumination and slow current recovery in dark. Our results in Figure 6 show a dramatically faster current recovery and higher sensitivity as long as the lamp energy is increased. For instance, a comparison between 365 nm (~3.0 eV) and 180 nm (~6.9 eV) exhibits one-fold faster response time (t_{90} from 70 to 6 s) and improved sensitivity from −4 to −28 percent response (% R)[57] for just double the energy applied to G. We believe that at high illumination energy ~6.9 eV, reactive O_2 species (ROS) are preferentially formed on the surface. It is known that oxygen radicals evolve at energies below 200 nm, therefore higher sensitivity (larger

dx.doi.org/10.1021/am405753t | ACS Appl. Mater. Interfaces XXXX, XXX, XXX−XXX

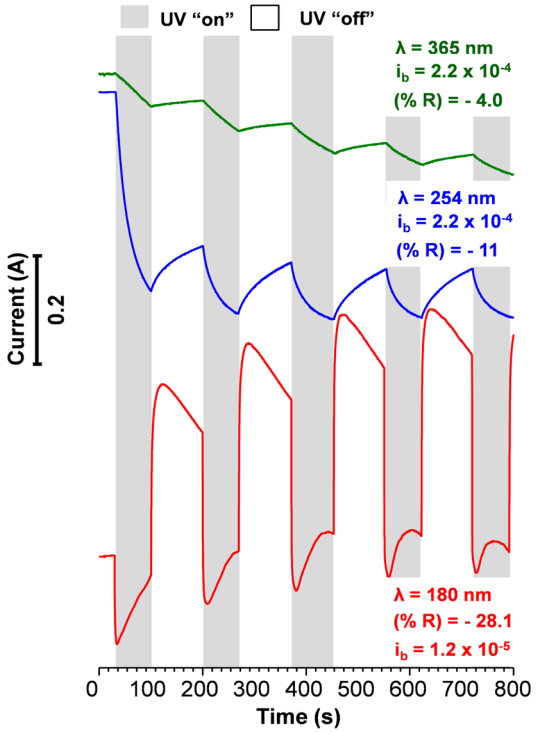

Figure 6. Normalized CA plots of as-transferred G onto microelectrodes subjected to different UV wavelengths (365, 254, and 180 nm) along percent change in conductivity (% R) and G baseline current (i_b) as indicated. Plots are offset for better comparison.

decrease in current) could be attributed to larger amounts of desorbed species. During current recovery, one may consider the same paradigm where highly unstable species take shorter time to re-adsorb back onto graphene. More experiments will be conducted in order to better elucidate the sensing mechanism. Surface oxidation of G with O_3 and the heterojunction formation (with Au NPs) had no major effect on UV sensing as demonstrated in Supporting Information Figure S10 and S11, respectively.

CONCLUSIONS

In conclusion, we demonstrated that CVD grown G method yielded to a monolayer carbon thick film as indicated by Raman experiments. The film exhibited conductivity between 10^{-4} and 10^{-6} A however, we found that PMMA changed the electronic properties of G and remained as a residue even after conventional cleaning procedures. The G film demonstrated the ability to be spontaneously decorated with surfactant-coated Au NPs for LSPR characterization and Raman applications. It was determined that the heterojunction is a great platform for quenching FL and PL and improving the Raman signal of RhB. We showed that graphene is mainly responsible for quenching PL and FL while the heterojunction improved by more than 3-fold the Raman activity of RhB. Finally, although the different sensing profiles observed at different UV energies are not fully understood, it seems to be associated with oxygen species on the surface of graphene accompanied by the distortion of π-electrons cloud. In the future, we will incorporate graphene-coated Ag nanostructures in order to improve SERS activity of various Raman active molecules.

ASSOCIATED CONTENT

Supporting Information

Characterization of high quality graphene by XPS and Raman; the presence of PMMA observed by FTIR, XPS, and refractive index; LSPR of Au NPs on ITO; calculating photoluminescence spectra, TGA, and FTIR for knowing the temperature and percent at which the organic desorbs; AFM images of the heterojunction before and after thermal treatment; $I-V$ curves of oxidized graphene; the effects of different laser energies on graphene; and chronoamperometry plots for oxidized graphene and the heterojunction upon UV illumination. This material is available free of charge via the Internet at http://pubs.acs.org.

AUTHOR INFORMATION

Corresponding Author

*E-mail: fjiban@inifta.unlp.edu.ar.

Present Address

⊥(M.M.) Case Western Reserve University, Cleveland, Ohio 44106, United States

Notes

The authors declare no competing financial interest.

ACKNOWLEDGMENTS

We gratefully acknowledge financial support from projects PICT-PRH 295 and International Cooperation Projects (CONICET-NSF) with Dr. Zamborini at the University of Louisville. R.C.S. acknowledges PICT 2554. G.I.L. acknowledges projects PICT-324 and PME (2006) 1544. F.J.I. and M.C.D. thank Gustavo Gimenez from INTI for helping in the construction of microelectrodes and with SEM images of the heterojunction. M.C.D. acknowledges Aldo Rubert (INIFTA) for fruitful discussion about XPS and Eduardo Prieto (INIFTA) for technical support in AFM. M.C.D. acknowledges CCT-CONICET project for traveling to Córdoba (Argentina) to perform Raman Spectroscopy.

REFERENCES

(1) Schedin, F.; Geim, A. K.; Morozov, S. V.; Hill, E. W.; Blake, P.; Katsnelson, M. I.; Novoselov, K. S. *Nat. Mater.* **2007**, *6*, 652−655.
(2) Bonaccorso, F.; Sun, Z.; Hasan, T.; Ferrari, A. C. *Nat. Photonics* **2010**, *4*, 611−622.
(3) Xu, W.; Mao, N.; Zhang, J. *Small* **2013**, *9*, 1206−1224.
(4) Ferrari, A. C.; Meyer, J. C.; Scardaci, V.; Casiraghi, C.; Lazzeri, M.; Mauri, F.; Piscanec, S.; Jiang, D.; Novoselov, K. S.; Roth, S.; Geim, A. K. *Phys. Rev. Lett.* **2006**, *97*, 187401.
(5) Hummers, W. S.; Offeman, R. E. *J. Am. Chem. Soc.* **1958**, *80*, 1339−1339.
(6) Sidorov, A. N.; Sławiński, G. W.; Jayatissa, A. H.; Zamborini, F. P.; Sumanasekera, G. U. *Carbon* **2012**, *50*, 699−705.
(7) Li, X.; Zhu, Y.; Cai, W.; Borysiak, M.; Han, B.; Chen, D.; Piner, R. D.; Colombo, L.; Ruoff, R. S. *Nano Lett.* **2009**, *9*, 4359−4363.
(8) Dan, Y.; Lu, Y.; Kybert, N. J.; Luo, Z.; Johnson, A. T. C. *Nano Lett.* **2009**, *9*, 1472−1475.
(9) Huh, S.; Park, J.; Kim, Y. S.; Kim, K. S.; Hong, B. H.; Nam, J.-M. *ACS Nano* **2011**, *5*, 9799−9806.
(10) Sarantopoulou, E.; Kollia, Z.; Cefalas, A. C.; Manoli, K.; Sanopoulou, M.; Goustouridis, D.; Chatzandroulis, S.; Raptis, I. *Appl. Surf. Sci.* **2008**, *254*, 1710−1719.
(11) Pirkle, A.; Chan, J.; Venugopal, A.; Hinojos, D.; Magnuson, C. W.; McDonnell, S.; Colombo, L.; Vogel, E. M.; Ruoff, R. S.; Wallace, R. M. *Appl. Phys. Lett.* **2011**, *99*, 122108.
(12) Lim, Y.-D.; Lee, D.-Y.; Shen, T.-Z.; Ra, C.-H.; Choi, J.-Y.; Yoo, W. J. *ACS Nano* **2012**, *6*, 4410−4417.

(13) Lin, Y.-C.; Lu, C.-C.; Yeh, C.-H.; Jin, C.; Suenaga, K.; Chiu, P.-W. *Nano Lett.* **2011**, *12*, 414−419.
(14) Lin, Y.-C.; Jin, C.; Lee, J.-C.; Jen, S.-F.; Suenaga, K.; Chiu, P.-W. *ACS Nano* **2011**, *5*, 2362−2368.
(15) Fleischmann, M.; Hendra, P. J.; McQuillan, A. J. *Chem. Phys. Lett.* **1974**, *26*, 163−166.
(16) Stiles, P. L.; Dieringer, J. A.; Shah, N. C.; Van Duyne, R. P. *Annu. Rev. Anal. Chem.* **2008**, *1*, 601−626.
(17) Jensen, L.; Aikens, C. M.; Schatz, G. C. *Chem. Soc. Rev.* **2008**, *37*, 1061−1073.
(18) Zrimsek, A. B.; Henry, A.-I.; Van Duyne, R. P. *J. Phys. Chem. Lett.* **2013**, *4*, 3206−3210.
(19) Nie, S.; Emory, S. R. *Science* **1997**, *275*, 1102−1106.
(20) Reents, B.; Plieth, W.; Macagno, V. A.; Lacconi, G. I. *J. Electroanal. Chem.* **1998**, *453*, 121−127.
(21) Cortés, E.; Etchegoin, P. G.; Le Ru, E. C.; Fainstein, A.; Vela, M. E.; Salvarezza, R. C. *J. Am. Chem. Soc.* **2013**, *135*, 2809−2815.
(22) Camden, J. P.; Dieringer, J. A.; Zhao, J.; Van Duyne, R. P. *Acc. Chem. Res.* **2008**, *41*, 1653−1661.
(23) Lee, K.; Irudayaraj, J. *Small* **2013**, *9*, 1106−1115.
(24) McLellan, J. M.; Siekkinen, A.; Chen, J.; Xia, Y. *Chem. Phys. Lett.* **2006**, *427*, 122−126.
(25) Malinsky, M. D.; Kelly, K. L.; Schatz, G. C.; Van Duyne, R. P. *J. Am. Chem. Soc.* **2001**, *123*, 1471−1482.
(26) Wilcoxon, J. P.; Martin, J. E.; Parsapour, F.; Wiedenman, B.; Kelley, D. F. *J. Chem. Phys.* **1998**, *108*, 9137−9143.
(27) Hasegawa, T.; Nishijo, J.; Umemura, J. *Chem. Phys. Lett.* **2000**, *317*, 642−646.
(28) Yu, X.; Cai, H.; Zhang, W.; Li, X.; Pan, N.; Luo, Y.; Wang, X.; Hou, J. G. *ACS Nano* **2011**, *5*, 952−958.
(29) Liu, J.; Cai, H.; Yu, X.; Zhang, K.; Li, X.; Li, J.; Pan, N.; Shi, Q.; Luo, Y.; Wang, X. *J. Phys. Chem. C* **2012**, *116*, 15741−15746.
(30) Murphy, S.; Huang, L.; Kamat, P. V. *J. Phys. Chem. C* **2013**, *117*, 4740−4747.
(31) Dutta, S.; Ray, C.; Sarkar, S.; Pradhan, M.; Negishi, Y.; Pal, T. *ACS Appl. Mater. Interfaces* **2013**, *5*, 8724−8732.
(32) Chen, P.; Yin, Z.; Huang, X.; Wu, S.; Liedberg, B.; Zhang, H. *J. Phys. Chem. C* **2011**, *115*, 24080−24084.
(33) Kim, Y.-K.; Han, S. W.; Min, D.-H. *ACS Appl. Mater. Interfaces* **2012**, *4*, 6545−6551.
(34) Saito, R.; Dresselhaus, G.; Dresselhaus, M. S. *Physical Properties of Carbon Nanotubes*; Imperial College Press: London, 1998.
(35) Fink, J.; Kiely, C. J.; Bethell, D.; Schiffrin, D. J. *Chem. Mater.* **1998**, *10*, 922−926.
(36) Dalfovo, M. C.; Salvarezza, R. C.; Ibañez, F. J. *Anal Chem.* **2012**, *84*, 4886−4892.
(37) Sidorov, A. N.; Sherehiy, A.; Jayasinghe, R.; Stallard, R.; Benjamin, D. K.; Yu, Q.; Liu, Z.; Wu, W.; Cao, H.; Chen, Y. P.; Jiang, Z.; Sumanasekera, G. U. *Appl. Phys. Lett.* **2011**, *99*, 013115.
(38) Wallace, P. R. *Phys. Rev.* **1947**, *71*, 622−634.
(39) $\sigma = (1/\rho)$ (A/d). Where, σ = conductivity ($1/\Omega\cdot$m); ρ = resistivity ($\Omega\cdot$m); A = cross-section (m^2); d = length between Au electrodes (m).
(40) Ibañez, F. J.; Zamborini, F. P. *ACS Nano* **2008**, *2*, 1543−1552.
(41) Rechberger, W.; Hohenau, A.; Leitner, A.; Krenn, J. R.; Lamprecht, B.; Aussenegg, F. R. *Opt. Commun.* **2003**, *220*, 137−141.
(42) Mie, G. *Ann. Phys.* **1908**, *25*, 377.
(43) Templeton, A. C.; Pietron, J. J.; Murray, R. W.; Mulvaney, P. *J. Phys. Chem. B* **2000**, *104*, 564−570.
(44) Izquierdo-Lorenzo, I.; Kubackova, J.; Manchon, D.; Mosset, A.; Cottancin, E.; Sanchez-Cortes, S. *J. Phys. Chem. C* **2013**, *117*, 16203−16212.
(45) Mooradian, A. *Phys. Rev. Lett.* **1969**, *22*, 185−187.
(46) Liao, H.; Wen, W.; Wong, G. K. *J. Opt. Soc. Am. B* **2006**, *23*, 2518.
(47) Smith, B. L.; Hutchison, J. E. *J. Phys. Chem. C* **2013**, *117*, 25127−25137.
(48) Maye, M. M.; Zhong, C.-J. *J. Mater. Chem.* **2000**, *10*, 1895−1901.
(49) Hoggard, A.; Wang, L.-Y.; Ma, L.; Fang, Y.; You, G.; Olson, J.; Liu, Z.; Chang, W.-S.; Ajayan, P. M.; Link, S. *ACS Nano* **2013**, *7*, 11209−11217.
(50) Costa, S. D.; Righi, A.; Fantini, C.; Hao, Y.; Magnuson, C.; Colombo, L.; Ruoff, R. S.; Pimenta, M. A. *Solid State Commun.* **2012**, *152*, 1317−1320.
(51) Shi, Y.; Fang, W.; Zhang, K.; Zhang, W.; Li, L.-J. *Small* **2009**, *5*, 2005−2011.
(52) Chen, R. J.; Franklin, N. R.; Kong, J.; Cao, J.; Tombler, T. W.; Zhang, Y.; Dai, H. *Appl. Phys. Lett.* **2001**, *79*, 2258−2260.
(53) Ryu, S.; Liu, L.; Berciaud, S.; Yu, Y.-J.; Liu, H.; Kim, P.; Flynn, G. W.; Brus, L. E. *Nano Lett.* **2010**, *10*, 4944−4951.
(54) Luo, Z.; Pinto, N. J.; Davila, Y.; Johnson, A. T. C. *Appl. Phys. Lett.* **2012**, *100*, 253108−4.
(55) Dinh, T.; Shon, Y.-S. *ACS Appl. Mater. Interfaces* **2009**, *1*, 2699−2702.
(56) Lin, J.; Zhong, J.; Kyle, J. R.; Penchev, M.; Ozkan, M.; Ozkan, C. S. *Nanotechnology* **2011**, *22*, 355701.
(57) % Response = $(i_r - i_b)/i_b \times 100 = \Delta i/i_b \times 100$, where i_r is the current response and i_b is the baseline current.